ADVANCED MATERIALS INTERFACES
www.advmatinterfaces.de

Probing the Edges between Stability and Degradation of a Series of ZnSe-Based Layered Hybrid Semiconductors

*Mengwen Yan, Christopher A. Myers, Gregory M. John, Vincent E. Meyers, Alan A. Chen, and Jeremy I. Feldblyum**

The discovery of layered materials with potentially unique electrical and chemical properties has become a major focus of materials research in the past decade. 2D II–VI layered hybrids (LHs) are a family of ligand-protected layered materials capable of isolation in few-layer form and possess emissive and electronic properties of potential relevance to semiconductor device technologies. The authors showed previously that, akin to black phosphorus and transition metal dichalcogenides, 2D II–VI LHs are sensitive to ambient atmospheric conditions. However, the causes for degradation of these ligand-protected materials remain unclear. Using ZnSe-based LHs, it is shown herein that the stability of these materials is related to the length and chemistry of the organic ligands coordinated to the LH surfaces. Furthermore, exposure to isotopically enriched $H_2{}^{18}O$ and $^{18}O_2$ reveals that H_2O and O_2 are both reactants contributing to ZnSe-LH degradation. An H_2O-initiated degradation pathway is proposed and is supported by density functional theory calculations. The findings contribute to the discovery of protection strategies for layered materials and elucidate a degradation pathway that may also be applicable to other layered materials.

1. Introduction

2D II–VI layered hybrids (LHs) are a class of crystalline inorganic–organic hybrid materials with the general formula (MQ)L, where M = Zn, Mn, or Cd, Q = S, Se, or Te, and L is typically a primary aliphatic monoamine.[1] Each hybrid layer, which contains an inorganic slab capped by organic ligands, is associated with neighboring layers only by van der Waals forces. Quantum confinement[2] of the quasi-2D inorganic slab leads to wide band-gaps (typically in the range of 3–4.5 eV), lending these materials potential for applications such as white light-emitting diodes and fluorescence-based sensors.[1c,3] Some computational studies have also predicted high hole and electron mobilities and efficient excited state photoemission due to high exciton binding energies.[2] Finally, they have been calculated[4] and measured[5] to exhibit unusually low thermal conductivity, a promising characteristic for use in thermoelectric devices. However, like many other 2D materials (e.g., black phosphorus [BP],[6] transition metals dichalcogenides [TMDCs],[7] and bismuthine[8]), 2D II–VI LHs also exhibit a propensity toward oxidation after long-term exposure to air, which limits their (opto)electronic performance as exfoliated few-layer material. In contrast to typical 2D materials, 2D II–VI LHs possess organic ligands coordinated to each layer, potentially providing a natural means with which to control these materials' ambient stability. In an initial study, we found that for an archetypal ZnSe-based LH, stability appears to be related to the length of the organic ligands bound to each layer.[9] The ligand also impacts the materials' stability during and after exfoliation by shear mixing.[9]

It has been demonstrated that passivation of BP[10] and TMDCs[11] with organic molecules can significantly improve their chemical stability in the presence of H_2O and O_2. In fact, 2D II–VI LHs can be regarded as inherently passivated 2D materials, with thin (<0.5 nm) inorganic layers passivated by chemically coordinated alkylamines of lengths up to 3.6 nm. However, to our knowledge, there has been no systematic study relating the stability of II–VI LHs with the identity of the surface-bound ligands. Furthermore, the mechanism of II–VI LH degradation is not fully understood.

M. Yan, C. A. Myers, G. M. John, A. A. Chen, J. I. Feldblyum
Department of Chemistry
The University at Albany
State University of New York
Albany, NY 12222, USA
E-mail: jfeldblyum@albany.edu
C. A. Myers
Department of Physics
The University at Albany
State University of New York
Albany, NY 12222, USA
C. A. Myers, G. M. John, A. A. Chen
The RNA Institute
University at Albany
State University of New York
Albany, NY 12222, USA
V. E. Meyers
College of Nanoscale Science and Engineering
State University of New York Polytechnic Institute
Albany, NY 12203, USA

The ORCID identification number(s) for the author(s) of this article can be found under https://doi.org/10.1002/admi.202200347.

DOI: 10.1002/admi.202200347

In this work, we seek to demonstrate the possibilities and limitations of protecting 2D II–VI LHs from ambient conditions with surface-bound ligands alone and elucidate the mechanism by which these materials degrade in air. We focus here on a series of previously unreported 2D II–VI LHs of the general composition ZnSe(L) (L = primary monoamine). The parent ZnSe has long been considered for blue-green diode lasers due to its band gap energy of 2.7 eV.[12] It has also been considered recently for energy storage applications.[13] In contrast to bulk ZnSe, the ZnSe(L) materials studied herein have orthorhombic lamellar structures and a wider bandgap (>4.0 eV). They are synthesized via ligand exchange from the readily accessible ZnSe(ba) (ba = n-butylamine). The relative stabilities of ZnSe(L) under ambient conditions are assessed by diffuse reflectance spectroscopy (DRS) and contact angle (CA) measurement. Longer linear alkylamine ligands lead to greater LH stability, where ligands possessing heteroatoms or cyclic functional groups provide a more complex picture of the role of ligands on LH stability. Exposure of LHs to isotopically enriched $H_2{}^{18}O$ and $^{18}O_2$ followed by characterization by dynamic secondary ion mass spectrometry (D-SIMS) allows us to propose a possible degradation mechanism for this class of materials. Density functional theory (DFT) calculations lend support to a proposed H_2O-initiated degradation pathway.

2. Results and Discussion

With the aim of better understanding the relationship between surface-bound ligand and LH stability, we synthesized a series of ZnSe(L) compounds having a variety of linear and nonlinear primary monoamine ligands. The identities and abbreviations of these ligands are shown in **Figure 1** and Scheme S1 (Supporting Information). We first attempted to synthesize these compounds solvothermally from $ZnCl_2$, Se, and the capping ligand. While success was achieved in several cases, we also observed some synthesis products to possess reduced crystallinity or coprecipitated elemental Se (Figure S2, Supporting Information). Furthermore, attempts to solvothermally synthesize the hypothetical ZnSe(amch) produced no solid whatsoever.

To reproducibly obtain phase-pure ZnSe(L) powders of sufficient crystallinity, we used a ligand-exchange approach. Powder samples of ZnSe(ba) were incubated at temperatures of 100 (for eea and bza ligands; vide infra) or 140 °C (for all other ligands) in neat ligand for 5 d under autogenous pressure. All samples synthesized by ligand exchange show powder patterns with sharp reflections and distinct from that of the parent ZnSe(ba) (Figure 1a,b). The three lowest angle reflections of each powder pattern, which are assigned to the (00*n*) family of planes, indicate the interlayer spacing (calculated with Bragg's law[14]) between the ZnSe basal planes enforced by the capping ligands

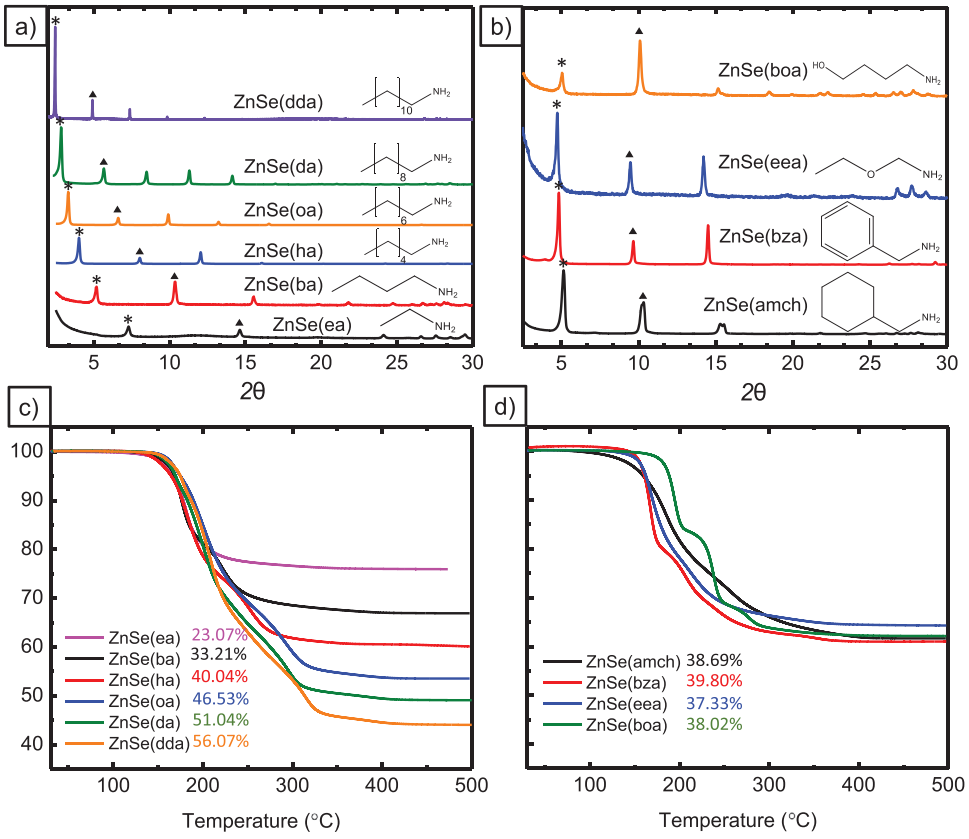

Figure 1. a,b) X-ray diffractograms of all materials synthesized by ligand exchange in this work. The star and triangle symbols refer to the (002) and (004) planes, respectively. c,d) Thermogravimetric analysis (TGA) of 2D II–VI LHs studied in this work. Mass loss of each sample from 30 to 500 °C is provided as a percentage value next to each sample identity in the figure legend.

Table 1. Interlayer distance between ZnSe basal planes in each 2D II–VI LH. The predicted distance (d_{model}, third column) is calculated from models constructed in silico from the parent ZnSe(ba) (see the Experimental Section for details). The measured interlayer distance (d_{exp}, fifth column) is obtained from the (002) reflection from the corresponding PXRD patterns. Percent error is calculated as $(d_{exp} - d_{model})/d_{model}$.

Materials	Theoretical 2θ at (002) plane	Theoretical d-spacing [nm]	2θ obtained from XRD pattern	Experimental d- spacing [nm]	Percent error
ZnSe(ea)	7.1920	1.2281	7.2800	1.2133	–1.2%
ZnSe(ba)	5.1561	1.7125	5.1680	1.7086	–0.2%
ZnSe(ha)	3.9690	2.2244	4.0279	2.1919	–1.5%
ZnSe(oa)	3.2493	2.7169	3.3130	2.6648	–1.9%
ZnSe(da)	2.7300	3.2336	2.8324	3.1168	–3.6%
ZnSe(dda)	2.3540	3.7500	2.4768	3.6138	–3.6%
ZnSe(amch)	4.7500	1.8589	5.1021	1.7306	–6.9%
ZnSe(bza)	4.7968	1.8407	4.8482	1.8212	–1.0%
ZnSe(eea)	4.5772	1.9290	4.7506	1.8803	–2.5%
ZnSe(boa)	4.7994	1.8397	5.0418	1.7608	–4.3%

in the ligand-exchanged LHs. The symmetry and structure of the ZnSe basal planes along the *a*- and *b*-crystallographic axes remain unchanged after ligand exchange.

To determine the structures of the ligand-exchanged materials, the lowest-angle peak, assigned to the (002) plane, was used to calculate the spacing between ZnSe layers (**Table 1**). Computational models of each compound were constructed (see the Experimental Section and Figure S3, Supporting Information), and experimental powder X-ray diffraction (PXRD) data were compared with these simulated models. Good agreement was found between the modeled (d_{model}) and experimentally observed (d_{exp}) distances between ZnSe layers (<5% deviation for all but one compound). For ZnSe(ea), ZnSe(ba), ZnSe(ha), and ZnSe(oa), excellent matches are found between d_{model} and d_{exp} (<2% deviation). When replacing ba with the longest alkylamines examined in this work, da and dda, d_{exp} is 4% less than d_{model}. We attribute this deviation to the simplicity of our model, which does not account for the possibility that the longer ligands may tilt to a greater extent than shorter ligands. Furthermore, gaps between longer ligands within the same ligand layer, left by residual unexchanged ba, would enable tilting of these longer ligands to a greater extent than evident in the idealized crystallographic model.[15] Such tilting would reduce interlayer spacing, accounting for the greater deviation between d_{exp} and d_{model} in these compounds (especially those possessing longer ligands).

Direct analysis in real time mass spectrometry (DART-MS)[16] was used to qualitatively examine the presence of the exchanged ligands (Figure S4, Supporting Information). All n-alkylamine substituted samples exhibit strong signals consistent with those expected for exchanged ligands (excepting ZnSe(ea), as the mass of ea is too low to observe in our instrument). Furthermore, only residual ba was observed for ZnSe(alkylamine) (<0.1% relative integrated intensity), indicating high ligand exchange yield (LEY) for those compounds. Thermogravimetric analysis (TGA) (Figure 1c,d) and elemental (CHN) microanalysis were used to independently quantify the achieved LEY. Equation S1 (Supporting Information) describes the method used to quantify LEY from TGA and CHN microanalysis. The results of both TGA measurements and CHN microanalysis are summarized in **Table 2**. Both methods show over 90% LEY in every n-alkylamine-exchanged compound. The high LEY in ZnSe(dda) suggests that we have not reached the limit of chain length that can be introduced into these materials via ligand exchange. Furthermore, these results show that the interlayer spacing can be adjusted at least over the range of 1.2–3.6 nm (ZnSe(ea) to (ZnSe(dda)).

The ligands containing cyclic groups, amch and bza, were more difficult to incorporate by exchange. A maximum of 75% of ba was exchanged with bza under the tested conditions. The low extent of ligand exchange in ZnSe(amch) is more pronounced: just 10%–40% of the ligand could be incorporated into the exchange product. Furthermore, the presence of multiple reflections where just one is expected (e.g., at 15.4° in 2θ, corresponding to the (006) plane; Figure 1b) suggests the coexistence of at least two phases with different interlayer spacing. Extending the ligand exchange incubation time of bza and amch led to samples exhibiting poor crystallinity and no increase in LEY. Analysis by DART-MS also reveals non-negligible signal intensity attributable to the presence of ba in these samples, consistent with only partial exchange. We

Table 2. Extent of ligand exchange (x) obtained for all 2D II–VI LHs studied in this report. Error bars represent one standard deviation from the mean ($N = 3$). Data for CHN analysis represent the range (minimum and maximum) obtained from two separate measurements of each compound.

Compound	x (by TGA)	x (by CHN analysis)
$ZnSe(ba)_{1-x}(ea)_x$	0.978 ± 0.013	0.9691–0.9707
$ZnSe(ba)_{1-x}(ha)_x$	0.939 ±0.006	0.9510–0.9790
$ZnSe(ba)_{1-x}(oa)_x$	0.937 ± 0.010	0.9927–0.9973
$ZnSe(ba)_{1-x}(da)_x$	0.944 ± 0.022	0.8892–0.9054
$ZnSe(ba)_{1-x}(dda)_x$	0.988 ± 0.002	0.9611–0.9695
$ZnSe(ba)_{1-x}(amch)_x$	0.393 ± 0.043	0.1333–0.1463
$ZnSe(ba)_{1-x}(bza)_x$	0.752 ± 0.092	0.7420–0.7425
$ZnSe(ba)_{1-x}(eea)_x$	0.942 ± 0.054	0.9528–0.9673
$ZnSe(ba)_{1-x}(boa)_x$	0.939 ± 0.038	0.9582–0.9707

posit that the larger footprint of bza and amch on the surface of the ZnSe slab limits the extent to which these ligands can substitute ba. Between these two ligands, the planarity of the aromatic bza enables somewhat greater LEY for this ligand compared to the non-planar amch. Models of fully substituted ZnSe(bza) and ZnSe(amch) exhibit different extents of distortion in the ZnSe layer (Figure S5, Supporting Information). The Zn—Zn distance within the basal plane, a descriptor of the distance between ligands on the plane surface, increases by 9% for both models. Changes in Zn—Se—Zn bond angles deviate an average of 4% in ZnSe(bza) from those of ZnSe(ba); the corresponding deviation in ZnSe(amch) is a much greater 14%. These models are consistent with the observation of low LEY in ZnSe(bza) and lower LEY in ZnSe(amch), and illustrate that unfavorable basal plane distortion prevents complete transformation of ZnSe(ba) to pure ZnSe(bza) or ZnSe(amch).

Compounds formed from ligand exchange with oxygen-incorporated ligands (eea and boa) exhibit PXRD patterns in agreement with those of simulated models. The predicted interlayer distance (d_{model}) of ZnSe(eea) deviates only 2.5% from the experimental d_{exp}, and a deviation of 4.3% is found between these parameters for ZnSe(boa). TGA and CHN analysis show a high LEY (ca. 95%) for these two materials.

ZnSe-based LHs exhibit a propensity to oxidize over time under ambient conditions. We previously showed that degradation of ZnSe(ba) in air produces Se nanoparticles and ZnO.[9] The Se nanoparticles produced from degradation have a dark red color; as such, they reduce the white-light reflectance of the degrading LH sample.[17] This color change can be quantified by DRS.

To quantify the relative stabilities of the II–VI LHs synthesized in this work, samples were sealed in two glass enclosures. In the first enclosure, the relative humidity (RH) was fixed at 50% using a saturated aqueous solution of $MgNO_3$ (referred hereafter as the "humid environment"). The second enclosure was charged with sufficient molecular sieve to maintain a RH below 1%[18] (referred to hereafter as the "dry environment"). Both enclosures were sealed in air and left at room temperature (22–23 °C) for the duration of the experiment. Samples were analyzed by DRS every 5 d over a period of 30 d to assess degradation over time (using color change as a relative indication of degradation). The normalized average of diffuse reflectance in the visible region (400–700 nm) for samples in the humid environment is shown in **Figure 2**a. To assess the impact of hydrophilicity on the rate of degradation, CA measurements were also carried out before and after the 30 d of exposure to humid and dry environments (Figure 2b and Figure S10c,d, Supporting Information).

Exposure of II–VI LHs to the humid environment led to pronounced reductions in both contact angle and white light reflectance over the course of 30 d. Among n-alkylamine-containing LHs, the degradation rate followed the order (from highest to lowest) ZnSe(ea) > ZnSe(ba) > ZnSe(ha) > ZnSe(oa) > ZnSe(da) > ZnSe(dda), in accordance with our hypothesis that longer chains protect the inorganic layers more so than shorter chains. The II–VI LH with the longest ligand tested

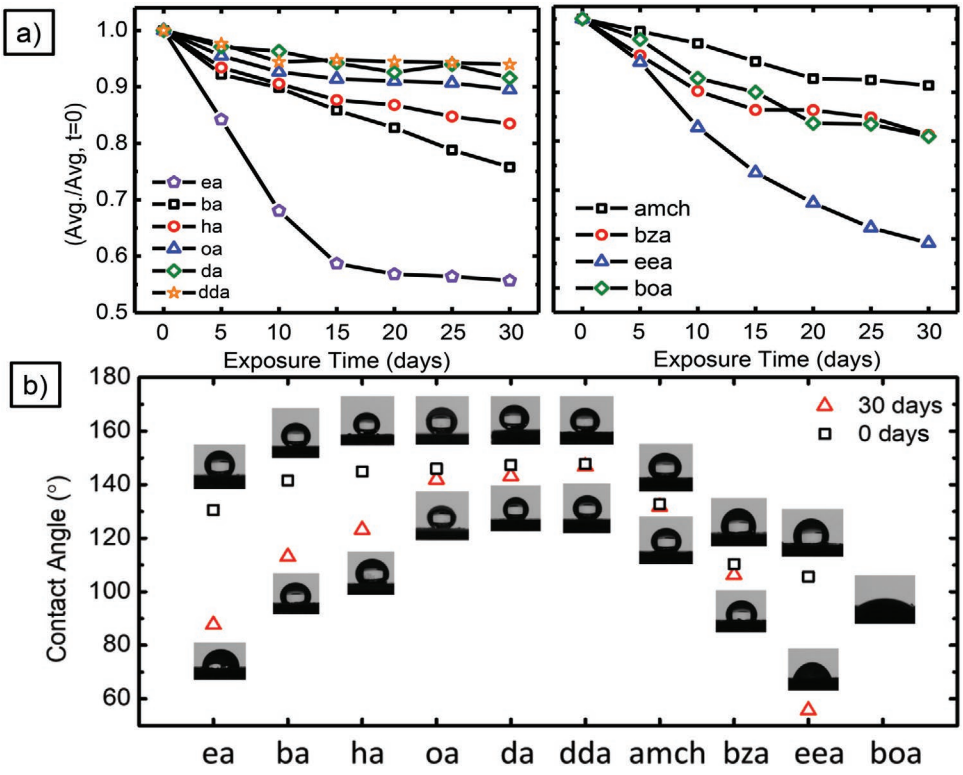

Figure 2. a) Normalized average of diffuse reflectance in the visible region (400–700 nm) of all ligand-exchanged LHs over a period of 30 d in a 50% RH, room temperature environment. b) Contact angle measurement of all ligand-exchanged samples before and after 30 d in a 50% RH, room temperature environment.

here, dda, exhibited a reduction in visible light reflectance of just 6% after 30 d [compared with a change of 25% for the ba-containing ZnSe(ba)] and a change in CA of just 1° [compared with a change of 28° for ZnSe(ba)] after being held in the humid environment. Similar trends were observed for alkane-protected BP[10a] and Ge nanowires.[19] We reason that increasing chain length reduces diffusion rates for O_2 and H_2O, reducing LH degradation rate. However, the ligand length alone is not fully predictive of degradation rate. For example, ZnSe(eea) and ZnSe(boa) both possess ligands of lengths similar to that of n-pentylamine. The degradation of ZnSe(boa) is consistent with that expected given its ligand chain length: after 30 d in the humid environment, it exhibited a decrease in white light reflectance to 80% of the original value, between those of the shorter-chain ZnSe(ba) (76%) and the longer-chain ZnSe(ha) (84%). In contrast, both DRS and CA measurements of ZnSe(eea) exposed to the humid environment for 30 d showed degradation closer to that of ZnSe(ea). While the increased hydrophilicity of ZnSe(eea) compared to that of the LHs capped by n-alkylamines may play a role in its more-rapid-than-expected degradation, the highly hydrophilic ZnSe(boa) (CA < 10 °C) does not exhibit such rapid degradation. While the hydroxide groups terminating the boa ligand could stabilize the layer by coordinating to the ZnSe slab (instead of coordinating via the amine group), plane wave DFT calculations (Figures S6 and S7, Supporting Information) oppose this hypothesis. Ligand binding via the amine group is ≈50% more enthalpically favored over that via the hydroxyl group. Analysis by FTIR (Figure S8, Supporting Information) provided no indication of ligand binding mode. Hence, we used 1-heptanol as a ligand to exchange with ba in ZnSe(ba). The material obtained by incubating ZnSe(ba) in neat 1-heptanol at 140 °C for 5 d was analyzed by PXRD and thermogravimetric analysis (Figure S9, Supporting Information). As shown by PXRD (Figure S9a, Supporting Information), a complete transformation of ZnSe(ba) to an unknown phase occurs. While this new phase possesses crystallinity, all indication of lamellar ordering is lost [i.e., the (002), (004), and (006) reflections vanish]. Analysis by TGA (Figure S9b, Supporting Information) shows a mass loss of 44.86%, corresponding to a LEY > 99%. Hence, while coordination from hydroxyl groups is possible, it leads to structural transformation that is not observed in ZnSe(boa). We therefore contend that, consistent with DFT calculations, hydroxyl coordination does not have a significant presence in ZnSe(boa).

ZnSe(amch) and ZnSe(bza) present another case study on the influence of nonlinear ligands on LH stability. Despite the low LEY of ZnSe(amch) (10%–40%) and lack of phase purity, its white light reflectance falls to just 89% of the original value in the humid environment over 30 d compared with ZnSe(bza), whose white light reflectance falls to 81% under identical conditions. It is known that benzene forms hydrogen bonds with water;[20] hence, similar hydrogen bonding between the aromatic ring of bza and water is expected. The greater water affinity of ZnSe(bza) compared with that of ZnSe(amch) is supported by the initial CAs of these compounds (110° and 132°, respectively). We posit that the relative hydrophobicity imparted by amch compared with that of bza imposes a greater kinetic barrier towards H_2O interacting with the underlying ZnSe layer.

To test the influence of H_2O on LH degradation, we subjected all ligand-exchanged LHs to incubation in the dry environment. All materials stored this way exhibited relative changes of less than 10% in their white light reflectance characteristics (Figures S10a,b, Supporting Information) and less than 3% in their CAs (Figures S10c,d, Supporting Information) after 30 d. The limited degradation of these compounds in the dry environment compared to that observed after exposure to the humid environment show that H_2O plays an important role in the degradation of these LHs.

Layered materials such as BP and TMDCs are reported to be highly sensitive to environmental gases (O_2 and H_2O in particular),[21] and degradation becomes more rapid for thinner samples. However, the mechanism of their degradation remains an active subject of study, and numbers of distinct mechanisms have been proposed. For instance, some have attributed the degradation of BP to its hydrophilic surface;[22] others have identified a low barrier to oxygen dissociation and dangling edge O atoms as the primary drivers of degradation.[23] Furthermore, evidence for a photo-assisted oxidation mechanism has been reported.[24] While layered TMDCs such as MoS_2 have been suggested to be air-stable in their pristine form, in practice, degradation upon exposure to H_2O and O_2 is well-documented.[21] It has been suggested this reactivity can be attributed to edge defects, grain boundaries and surface vacancies.[25] Rapid degradation has also been observed in Se-containing TMDCs such as $TiSe_2$, $TaSe_2$, and $NbSe_2$.[26]

We have shown herein that, akin to BP and TMDCs, ZnSe-based II–VI LHs exhibit chemical sensitivity toward humid air. We showed previously that the degradation of these materials leads to the formation of Se and ZnO.[9] Limiting the presence of water mitigates this degradation (vide supra). Hence, water plays an important role in the degradation process. However, the role of water remains unclear, as the source of oxygen in the ZnO degradation product could either come from atmospheric O_2, similar to the reported degradation route of BP,[23] both H_2O and O_2, a route potentially similar to that of the corrosion of metals such as Fe,[27] or from the oxygen in H_2O alone. Exposure of ZnSe(ba) to a O_2-free, 50% RH environment led to the minor changes in both white light reflectance and CA comparable to those observed for ZnSe(ba) incubated in a dry environment (Figure S11, Supporting Information). Hence, *both* O_2 and H_2O play important roles in the degradation of ZnSe-based LHs. However, little mechanistic insight is provided by these experiments alone.

To better understand the roles of O_2 and H_2O in II–VI LH degradation, we used D-SIMS to track the source of oxygen in degraded LHs. ZnSe(ba), which degrades over relatively short time scales, was exposed to environments having isotopically enriched $H_2{}^{18}O$ or $^{18}O_2$. Three separate samples of ZnSe(ba) were exposed to environments of 50% RH having no isotopically enriched compounds, $H_2{}^{18}O$ as the source of water, or $^{18}O_2$ as the source of oxygen, respectively. These samples were left at ambient temperature for 10 d in their respective environments. The samples were then subjected to reduced pressure (≈0.01 Torr) to remove adsorbed species (e.g., $H_2{}^{18}O$ or $^{18}O_2$) prior to characterization with D-SIMS. Further experimental details are provided in Figure S12 (Supporting Information).

A summary of D-SIMS analysis results is shown **Figure 3**, with raw data shown in Figure S13 (Supporting Information).

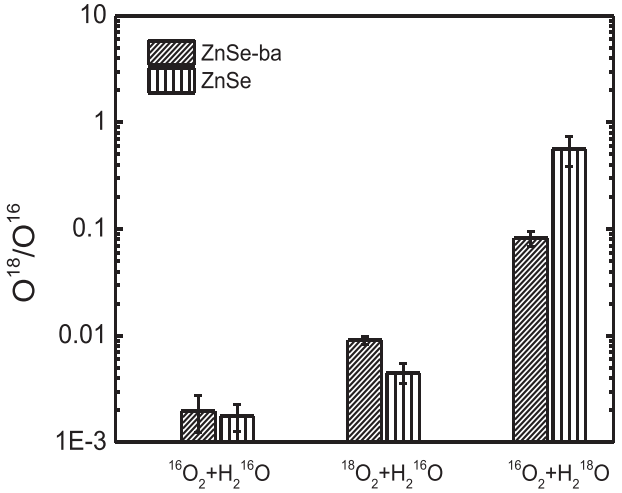

Figure 3. D-SIMS analysis of ZnSe(ba) exposed to naturally abundant H_2O and O_2 or to environments having either $H_2{}^{18}O$ or $^{18}O_2$ as described in the main text. Values shown are averages from three depth-profile measurements, each averaged over 2-min acquisitions (Figure S13, Supporting Information). Error bars represent one standard deviation from the mean.

Each bar depicts the mean and standard deviation of three depth profiles, each measured over 120 s of sputtering. ZnSe(ba) treated with non-isotopically enriched H_2O and O_2 exhibited a $^{18}O/^{16}O$ ratio nearly identical to the natural isotopic abundance ratio of 0.204%, confirming that the ratio of the mass measurements corresponds to the ratio of O isotope present in the material.[28] When isotopically labeled $^{18}O_2$ was used in place of naturally abundant O_2, the $^{18}O/^{16}O$ ratio increased by a factor of 4–5 times to 0.9%. This result supports the hypothesis that oxygen atoms from O_2 are part of the ZnO degradation product. Depth profiles of ZnSe(ba) exposed to $H_2{}^{18}O$ in the presence of naturally abundant O_2 yield an average $^{18}O/^{16}O$ ratio of 8.0%, nearly 20 times higher than that detected in sample exposed to naturally abundant H_2O and O_2. Hence, H_2O is also an important reactant in the degradation of these materials and does not merely act as a catalyst. We rule out the possibility that the high $^{18}O/^{16}O$ signal may come from residual water at the sample surface based on consistent $^{18}O/^{16}O$ signal intensity during the entire 2 min etching frame (Figure S13, Supporting Information). While the roughness of drop-cast ZnSe(ba) powder films precluded quantification of sputtering depth during D-SIMS, sputtering of the more dense ZnSe suggests an upper limit to the depth profiled in our D-SIMS experiment of ≈1 µm.

To better understand the role of the ligand on LH degradation, ZnSe was exposed to isotopically enriched environments identical to those used for ZnSe(ba) degradation and analyzed by D-SIMS. Exposure to isotopically enriched $^{18}O_2$ yielded a similar 4–5-fold increase in the degraded material's $^{18}O/^{16}O$ ratio. However, ^{18}O incorporation from $H_2{}^{18}O$ was ≈5 times greater than that observed for ZnSe(ba). For the same degradation mechanism, the amount of ^{18}O contributed from $^{18}O_2$ and $H_2{}^{18}O$ should not change between the LH and the bulk material. As several different degradation pathways are available to ZnSe on exposure to H_2O and O_2,[29] we hypothesize that the surface-bound ba ligands of ZnSe(ba) restrict the number of roles H_2O can play in degradation, reducing the extent of incorporation of oxygen from H_2O.

With the aid of DFT calculations, we now propose one possible mechanism of degradation of ZnSe LHs. As previously reported scanning electron diffraction measurements suggest that degradation occurs from the basal plane edge,[9] we simulated a single layer fragment of ZnSe(L) (**Figure 4**, State 1) and calculated the enthalpy of water adsorption at this edge (Figure 4, State 2). The energy difference between the pristine fragment and that with water adsorbed is –99.2 kJ mol^{-1}, suggesting such adsorption is quite favorable. To degrade the material, both H_2O and O_2 must dissociate (eventually yielding the degradation product ZnO); we therefore hypothesize that H_2O dissociates at the basal plane edge to form OH^- and H^+, which become directly bound to the LH (Figure 4, State 3). The formation of OH^- in particular is quite plausible given the close

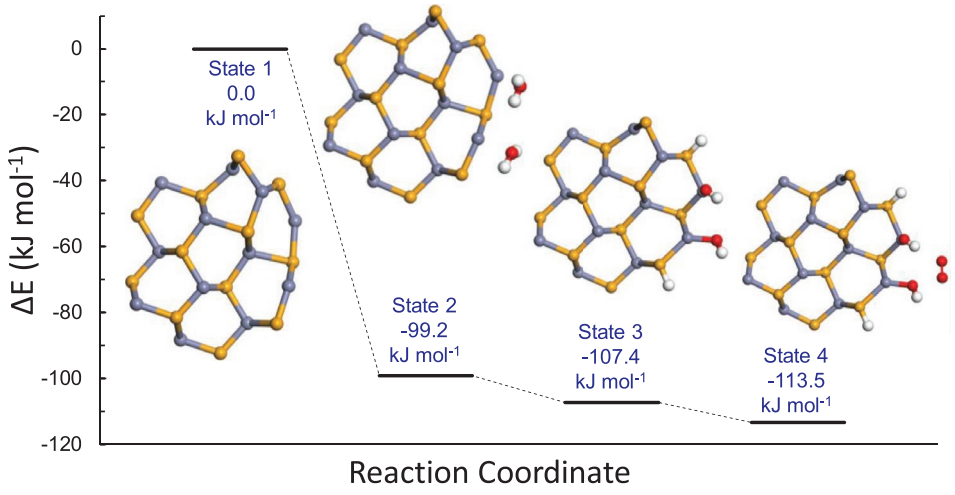

Figure 4. Proposed pathway for initiation of ZnSe(L) degradation by H_2O and corresponding relative energy diagram. Calculation includes water adsorption, dissociation, and dioxygen adsorption. Color scheme: Se, orange; Zn, grey; O, red; H, white. Ligands omitted for clarity.

proximity of the capping amines. These amines may serve as proton acceptors, mediating the formation of OH^- that can then bind to the Zn ions of the ZnSe fragment.[30] Furthermore, we observed experimentally that exposure of ZnSe(ba) to pH 6.8 water reduced its degradation rate; water of pH 7.0 or 7.2 led to more rapid degradation, suggesting that OH^- and not H^+ is critical for LH degradation. Dissociation of H_2O is exothermic with an energy difference of –8.2 kJ mol^{-1} before and after dissociation (Figure 4). Adsorption of oxygen at the fragment is then necessary to drive degradation; this too is exothermic by –6.1 kJ mol^{-1} (Figure 4, State 4). We propose the next step involves the oxidation of Se^{2-} by O_2, producing elemental Se^0 and $Zn(OH)_2$ (incorporating O from both H_2O and O_2). Directly simulating this process would be challenging due to the unphysical, transient nature of the lone Se^0 atoms and $Zn(OH)_2$ molecules that would be produced in the minimal supercell used for DFT calculations. Nonetheless, the chemical plausibility of this step is supported by the difference in redox potentials of ZnSe oxidation[31] [Equation (1)] and O_2 reduction[32] [Equation (2)]

$$Se^0 + Zn^{2+} + 2e^- \rightleftharpoons ZnSe\,(-0.459\ \text{V versus NHE}) \quad (1)$$

$$O_2 + 2H_2O + 4e^- \rightleftharpoons 4OH^-\ (+0.401\ \text{V versus NHE}) \quad (2)$$

The formation of $Zn(OH)_2$ from both O_2 and H_2O is also consistent with both of these gases behaving as reactants, as shown in our D-SIMS experiments (vide supra). Finally, ZnO can form spontaneously under ambient conditions from $Zn(OH)_2$ according to [Equation (3)][33]

$$Zn(OH)_2 \rightarrow ZnO + H_2O \quad (3)$$

3. Conclusion

In this work, we use a ligand exchange process to synthesize a series of ZnSe(L) LHs to elucidate the extent to which ligands can protect these compounds from degradation in ambient conditions, and to suggest a mechanism by which they degrade. ZnSe(L) with the linear ea, ba, ha, oa, da, dda, eea, and boa ligands can be successfully produced by ligand exchange with high (>90%) exchange yields. In contrast, cyclic amines bza and amch exhibit modest extents of ligand exchange. On exposure to humid environments, the longer alkylamine ligands slow degradation compared to the shorter ligands.

We also show that ZnSe(L) LHs degradation slows considerably when either O_2 or H_2O (or both) are excluded. Exposure of ZnSe(ba) to ^{18}O-enriched $H_2{}^{18}O$ and $^{18}O_2$ shows that the oxygen from both of these species is incorporated into the final ZnO degradation product. These data in conjunction with DFT calculations point to a degradation mechanism whereby water and oxygen are first reduced by Se^{2-} in the ZnSe layer to produce $Zn(OH)_2$ and Se^0, followed by spontaneous conversion of $Zn(OH)_2$ to ZnO over time.

These conclusions serve as a case study in both the protection and degradation of an archetypal quantum-confined 2D material. These results suggest approaches to protect other 2D materials, and may also provide relevant mechanistic steps to understand degradation in other TMDCs.

4. Experimental Section

Chemicals: Zinc nitrate hexahydrate (99% trace metals basis, Beantown Chemical), selenium powder (99%, Strem Chemicals), ethylamine (ea, 70% aqueous solution, VWR), n-butylamine (ba, 99+%, Acros Organics), n-hexylamine (ha, 99+%, Sigma-Aldrich) n-octylamine (oa, 99+%, Sigma-Aldrich), decylamine (da, 99+%, Sigma-Aldrich), dodecylamine (dda, 99+%, Sigma-Aldrich), aminomethylcyclohexane (amch, 98+%, TCI), benzylamine (bza, 99+%, TCI), 2-ethoxyethylamine (eea, 98+%, TCI), 4-amino-1-butanol (boa, 98+%, TCI), 1-heptanol (99%, Alfa Aesar), diethyl ether (anhydrous, J.T. Baker), magnesium nitrate hexahydrate (98%, Beantown Chemical), isotopically enriched water ($H_2{}^{18}O$, 97% isotopic enrichment, Cambridge Isotope Laboratories Inc.), zinc oxide (ZnO, 99.7%, Strem Chemicals Inc.), zinc selenide (ZnSe, ≈60 mesh powder, 99.99%, ALB Chemicals), and isotopically labeled dioxygen gas ($^{18}O_2$, Cambridge Isotope Laboratories, Inc. 97%) were used as received without further purification. Molecular sieves (3 Å, 1–2 mm beads, Beantown Chemical) were heated in a consumer grade microwave oven to remove adsorbed water prior to use.

Solvothermal Synthesis of ZnSe(ba): ZnSe(ba) was synthesized as described in a previous report.[34]

Solvothermal Synthesis of ZnSe(eea), ZnSe(bza), and ZnSe(da): To test the possibility of synthesizing these compounds directly, a method near-identical to that used for the synthesis of ZnSe(ba)[34] was used. The only differences were temperature, several of which were tested to optimize synthesis conditions, and the identity of the ligand. Temperatures of 100, 140, and 160 °C were tested. The final products were washed with pure ethanol and then acetone.

Exchange of Amine Ligands with ZnSe(ba): Dry ZnSe(ba) (50 mg, 0.22 mmol) was transferred to a 23 mL Teflon-lined autoclave, followed by addition of neat ligand (5 mL, 20–50 mmol). The autoclaves were sealed and heated under autogenous pressure at 140 °C for ea, ba, ha, oa, da, dda, bza, and boa. A temperature of 100 °C was used for amch and eea, as the lower temperature was found to yield samples of greater crystallinity and extent of ligand exchange. All ligand exchange reactions were performed over the course of 5 d. After 5 d, reactions were cooled under ambient conditions and the powder products were isolated by centrifugation, washed twice with pure ethanol (≈20 mL) and once with a 50:50 v:v mixture of ethanol and acetone. The samples were then dried under reduced pressure (≈0.01 Torr) for 1 d and stored in a N_2 glovebox until further analysis.

Exchange of 1-Heptanol with ZnSe(ba): Dry ZnSe(ba) (100 mg, 0.44 mmol) was mixed with 10 mL of 1-heptanol (70 mmol) in a 23 mL Teflon-lined autoclave. The autoclave was sealed and heated under autogenous pressure at 140 °C for 5 d. After this time, the reaction was cooled to room temperature. The product was then isolated by centrifugation and washed twice with ethanol, followed once with acetone. The final powder product was dried under reduced pressure (≈0.01 torr) at least 1 d prior to analysis by PXRD and TGA.

Powder X-Ray Diffraction: Powder X-ray diffractograms of all but one (vide infra) II–VI LHs were obtained with a D8 Advance X-ray powder diffractometer (Bruker Corp., Billerica, USA) using Cu Kα radiation. Measurements were performed with a step size of 0.02° (2θ) at a rate of 2 s/step at room temperature. Due to the low scattering angle of the (2 0 0) reflection of ZnSe(dda), powder data shown in Figure 1a for this compound were obtained at room temperature with synchrotron radiation (λ = 0.457901 Å) at beamline 11-BM of the Advanced Photon Source, Argonne National Laboratory. Further experimental details were described previously.[35]

Construction of Hypothetical Models of ZnSe(ea), ZnSe(ha), ZnSe(oa), ZnSe(da), ZnSe(dda), ZnSe(amch), ZnSe(bza), ZnSe(eea), and ZnSe(boa): Using ZnSe(ba) as a template, all hypothetical models were constructed in Materials Studio 8.0 (Biovia, San Diego, CA). Carbon, hydrogen, and oxygen atoms were either added to or subtracted from the initial ba chains until the chain was transformed to the appropriate ligand. The ZnSe basal plane was not modified in this process. The structure's geometry and unit cell parameters were then optimized using Forcite, a molecular mechanics-based module using the Universal Force Field.[36]

Force field parameters used in this work are identical to those described previously.[37]

Thermogravimetric Analyses: Thermogravimetric analysis was performed on Discovery TGA 5500 (TA Instruments, New Castle, USA). Samples were loaded into 100 µL platinum pans and heated with a ramp rate of 5 °C from 30 to 500 °C under flowing nitrogen. TRIOS software (TA Instruments) was used for data analysis.

Elemental Microanalyses (CHN Analysis): The C, H, and N contents of II–VI LHs were analyzed by a commercial contract laboratory (Atlantic Microlab Inc., Norcross, GA) using combustion methods.

Direct Analysis in Real Time Mass Spectrometry Analysis: A DART-SVP ion source (IonSense, Saugus, USA) combined with an AccuTOF mass spectrometer (JEOL USA Inc., Peabody, USA) was used for DART-MS analysis. The instrument was set to positive-ion mode and the gas heater was set to 300 °C. A m/z mass range of 40–800 was used. The DART ion source helium flow rate was 2.0 L min^{-1}, the orifice 1 voltage was 20 V, and the orifice 2 voltage was 5 V to minimize fragmentation. Poly(ethylene glycol) (PEG 600) was used to calibrate the mass spectra following sample analysis. TSSPro3 software (Schrader Analytical Laboratories, Detroit, USA) was used for mass spectral analysis.

Exposure of II–VI LHs to Controlled Environments: LH samples were dispersed from anhydrous ether onto Al foil discs (≈16 mm diameter). These samples were then placed in one of three environments and allowed to incubate at room temperature for 0–30 d. The dry environment consisted of a sealed desiccator filled with enough 3 Å molecular sieve to adsorb sufficient water from the desiccator.[18] The humid environment consisted of a sealed desiccator containing saturated aqueous $Mg(NO_3)_2$ (≈30 mL) to form a closed environment of 50% RH[38] at room temperature. To form an O_2-free closed environment of 50% RH, saturated aqueous $Mg(NO_3)_2$ (≈30 mL) was degassed by three freeze-pump-thaw cycles. The degassed solution was placed in a desiccator sealed within a N_2 atmosphere glovebox. For $H_2{}^{18}O/H_2{}^{16}O$ and $^{18}O_2/^{16}O_2$ isotope experiments, both ZnSe(ba) and ZnSe were placed in a 22 mL sealed container containing either 1 mL H_2O with ambient atmosphere, 1 mL $H_2{}^{18}O$ with otherwise ambient atmosphere, or H_2O (natural isotopic abundance) with $^{18}O_2$. ZnSe(ba) and ZnSe were exposed to these environments for 10 d at ambient temperature and with light excluded, after which samples were subject to reduced pressure (≈0.01 Torr) for no fewer than 2 d to remove adsorbed vapor or gas prior to analysis by D-SIMS.

Diffuse Reflectance Spectroscopy: DRS was carried out using a Jasco V-770 UV–vis–NIR spectrophotometer equipped with an integrating sphere attachment (ISV-922, 60 mm sphere diameter). After exposure to one of the controlled environments described above, samples were placed into a powder cell (Jasco PSH-002, 16 mm diameter) for analysis by DRS. Each DRS data point in Figure 2 and Figure S10 (Supporting Information) was obtained on separate independent samples to avoid delamination due to excessive handling of samples during time course measurements.

Contact Angle Measurement: CA measurement was performed using a contact angle goniometer (Ossila Inc., Sheffield, England). Powders of each sample were dispersed from anhydrous ether onto 1 × 1 cm rectangular silicon substrates. Dispersed samples were then exposed to one of the environments described above for 30 d at room temperature. The goniometer was calibrated using a calibration sphere under the manufacturer-specified focus distance before sample analysis. Measurements were obtained by recording 20 s videos. Contact angles were obtained by averaging the contact angle of each frame obtained in the video using the manufacturer's software.

Dynamic Secondary Ion Mass Spectrometry for Isotope Analysis: D-SIMS was performed using a Physical Electronics Phi 6650 using a Cs sputtering source. Measurements were obtained using a background pressure of 1.3×10^{-10} torr using a focused Cs beam rastered over a 500 µm × 500 µm area with a co-incident electron beam at 5 keV to prevent sample charging. At least three locations were sputtered for at least 120 s on each sample to assess the influence of localized surface or bulk compositional effects on the selected isotopic measurements.

DFT Calculations for H_2O and O_2 Involved Degradation of ZnSe(ba): DFT calculations were performed using Q-Chem 5.3.[39] The PBE0 density functional[40] was used to account for electron exchange and correlation energies in conjunction with the LANL2DZ effective core potential[41] to represent core electrons for Zn and Se atoms. The accompanying LANL2DZ basis set was also used during geometry optimization calculations, with additional polarization functions from the 6-31G* basis set[42] for O and N atoms. Final energies were then calculated without core potentials at the PBE0/pc-2 level of theory.[43] Dispersion interactions were incorporated using Grimme's D3 empirical correction.[44] A small fragment of ZnSe(ea) consisting of 12 Zn and 12 Se atoms and associated ligands was constructed from the reported crystal structure of ZnSe(ba)[34] (Figure 4 and Figure S14, Supporting Information). Geometries shown in Figure 4 are calculated as energy minimized structures using the default Q-Chem 5.3 search criteria. While States 1–3 were calculated with the conventional restricted Kohn-Sham DFT formalism, State 4 required a restricted open-shell calculation to correctly capture the triplet ground-state of molecular oxygen. To treat atoms remote to the site of degradation as "bulk" material, these atoms were fixed to the atomic positions found in the crystal structure during all geometry optimizations. Fixed atoms are shown graphically in Figure S14 (Supporting Information).

Supporting Information

Supporting Information is available from the Wiley Online Library or from the author.

Acknowledgements

The authors gratefully acknowledge support from the Donors of the American Chemical Society Petroleum Research Fund (No. 59835-DNI10 to J.I.F.) in partial support of this work, as well as startup funds provided by The University at Albany, State University of New York. A.A.C. acknowledges support from the National Science Foundation grant MCB-1651877. This work used the Extreme Science and Engineering Discovery Environment (XSEDE; allocation TG-MCB140273 to A.A.C.), which was supported by National Science Foundation Grant No. ACI-1548562. Support for thermogravimetry experiments was provided by National Science Foundation grant CHE-1919810. Use of the Advanced Photon Source at Argonne National Laboratory was supported by the U.S. Department of Energy, Office of Science, Office of Basic Energy Sciences, under Contract No. DE-AC02-06CH11357.

Conflict of Interest

The authors declare no conflict of interest.

Data Availability Statement

The data that support the findings of this study are available from the corresponding author upon reasonable request.

Keywords

2D materials, chemical stability, DFT calculations, dynamic secondary ion mass spectrometry, II–VI layered hybrids, mechanistic study

Received: February 14, 2022
Revised: May 4, 2022
Published online:

[1] a) X. Huang, J. Li, H. Fu, *J. Am. Chem. Soc.* **2000**, *122*, 8789; b) X. Huang, H. R. Heulings, J. Li, T. Yuen, C. L. Lin, *J. Nanosci. Nanotechnol.* **2005**, *5*, 1487; c) J. Li, R. Zhang, *Prog. Inorg. Chem.* **2011**, *57*, 445.
[2] a) S. Wei, J. Lu, Y. Qian, *Chem. Mater.* **2008**, *20*, 7220; b) H. Fu, J. Li, *J. Chem. Phys.* **2004**, *120*, 6721.
[3] a) W. Ki, J. Li, G. Eda, M. Chhowalla, *J. Mater. Chem.* **2010**, *20*, 10676; b) X. Fang, M. Roushan, R. Zhang, J. Peng, H. Zeng, J. Li, *Chem. Mater.* **2012**, *24*, 1710; c) M. Roushan, X. Zhang, J. Li, *Angew. Chem.* **2012**, *124*, 451; d) Y. Chen, J. Wang, J. Li, X. Li, S. Wei, *RSC Adv.* **2015**, *5*, 70238; e) T. Ye, M. Kocherga, Y.-Y. Sun, A. Nesmelov, F. Zhang, W. Oh, X.-Y. Huang, J. Li, D. Beasock, D. S. Jones, T. A. Schmedake, Y. Zhang, *ACS Nano* **2021**, *15*, 10565.
[4] X. Qian, X. Gu, R. Yang, *Nano Energy* **2017**, *41*, 394.
[5] X. Huang, M. Roushan, T. J. Emge, W. Bi, S. Thiagarajan, J.-H. Cheng, R. Yang, J. Li, *Angew. Chem., Int. Ed.* **2009**, *48*, 7871.
[6] G. Abellán, S. Wild, V. Lloret, N. Scheuschner, R. Gillen, U. Mundloch, J. Maultzsch, M. Varela, F. Hauke, A. Hirsch, *J. Am. Chem. Soc.* **2017**, *139*, 10432.
[7] a) C. R. Ryder, J. D. Wood, S. A. Wells, M. C. Hersam, *ACS Nano* **2016**, *10*, 3900; b) R. Yang, L. Mei, Q. Zhang, Y. Fan, H. S. Shin, D. Voiry, Z. Zeng, *Nat. Protoc.* **2022**, *17*, 358; c) Q. Zhang, L. Mei, X. Cao, Y. Tang, Z. Zeng, *J. Mater. Chem. A* **2020**, *8*, 15417.
[8] A. A. Kistanov, S. K. Khadiullin, K. Zhou, S. V. Dmitriev, E. A. Korznikova, *J. Mater. Chem. C* **2019**, *7*, 9195.
[9] M. Yan, S. M. Collins, P. A. Midgley, J. I. Feldblyum, *Chem. Mater.* **2020**, *32*, 2379.
[10] a) C. Su, Z. Yin, Q.-B. Yan, Z. Wang, H. Lin, L. Sun, W. Xu, T. Yamada, X. Ji, N. Zettsu, K. Teshima, J. H. Warner, M. Dincă, J. Hu, M. Dong, G. Su, J. Kong, J. Li, *Proc. Natl. Acad. Sci. USA* **2019**, *116*, 20844; b) C. R. Ryder, J. D. Wood, S. A. Wells, Y. Yang, D. Jariwala, T. J. Marks, G. C. Schatz, M. C. Hersam, *Nat. Chem.* **2016**, *8*, 597.
[11] a) S. A. Han, T. H. Kim, S. K. Kim, K. H. Lee, H. J. Park, J. H. Lee, S. W. Kim, *Adv. Mater.* **2018**, *30*, 1800342; b) X. Chen, A. R. McDonald, *Adv. Mater.* **2016**, *28*, 5738.
[12] D. D. Hile, H. C. Swart, S. V. Motloung, L. F. Koao, in *Nanoscale Compound Semiconductors and Their Optoelectronics Applications* (Eds: V. B. Pawade, S. J. Dhoble, H. C. Swart), Woodhead Publishing, Cambridge, MA **2022**.
[13] J. Jin, Y. Zheng, L. B. Kong, N. Srikanth, Q. Yan, K. Zhou, *J. Mater. Chem. A* **2018**, *6*, 15710.
[14] W. H. Bragg, W. L. Bragg, *Proc. R. Soc. London, Ser. A* **1913**, *88*, 428.
[15] a) Q. Zhang, F. Diao, X. Xue, X. Sheng, D. Barba, Y. Wang, *ACS Appl. Mater. Interfaces* **2021**, *13*, 44777; b) Z. Wang, X.-D. Wen, R. Hoffmann, J. S. Son, R. Li, C.-C. Fang, D.-M. Smilgies, T. Hyeon, *Proc. Natl. Acad. Sci. USA* **2010**, *107*, 17119; c) P. K. Ghorai, S. C. Glotzer, *J. Phys. Chem. C* **2010**, *114*, 19182.
[16] R. B. Cody, J. A. Laramée, H. D. Durst, *Anal. Chem.* **2005**, *77*, 2297.
[17] H. Chen, J.-B. Yoo, Y. Liu, G. Zhao, *Electron. Mater. Lett.* **2011**, *7*, 333.
[18] At 25 °C, moisture capacity of air is around 3.34 g cm^{-3}, the relative humidity (RH) in the lab is 40%, the volume of sealed container been used is 0.8 L, it can be estimated that the amount of water vapor in it is around 1.07×10^{-3} g. 100 g 3 Å molecular sieves was placed in each container, the adsoption capacity of it for a 40% RH water vapor in air at 25 °C is 20 g/100 g. In theory, all moisture should be absorbed by molecular sieves, and the RH should be close to 0%.
[19] D. Wang, Y.-L. Chang, Z. Liu, H. Dai, *J. Am. Chem. Soc.* **2005**, *127*, 11871.
[20] a) T. M. Raschke, M. Levitt, *J. Phys. Chem. B* **2004**, *108*, 13492; b) M. Levitt, M. F. Perutz, *J. Mol. Biol.* **1988**, *201*, 751; c) S. Burley, G. Petsko, *FEBS Lett.* **1986**, *203*, 139.
[21] Q. Li, Q. Zhou, L. Shi, Q. Chen, J. Wang, *J. Mater. Chem. A* **2019**, *7*, 4291.
[22] A. Castellanos-Gomez, L. Vicarelli, E. Prada, J. O. Island, K. Narasimha-Acharya, S. I. Blanter, D. J. Groenendijk, M. Buscema, G. A. Steele, J. Alvarez, *2D Mater.* **2014**, *1*, 025001.
[23] A. Ziletti, A. Carvalho, D. K. Campbell, D. F. Coker, A. C. Neto, *Phys. Rev. Lett.* **2015**, *114*, 046801.
[24] Q. Zhou, Q. Chen, Y. Tong, J. Wang, *Angew. Chem., Int. Ed.* **2016**, *55*, 11437.
[25] J. Gao, B. Li, J. Tan, P. Chow, T.-M. Lu, N. Koratkar, *ACS Nano* **2016**, *10*, 2628.
[26] L. Sun, C. Chen, Q. Zhang, C. Sohrt, T. Zhao, G. Xu, J. Wang, D. Wang, K. Rossnagel, L. Gu, C. Tao, L. Jiao, *Angew. Chem., Int. Ed.* **2017**, *56*, 8981.
[27] Z. Ahmad, *Principles of Corrosion Engineering and Corrosion Control*, Elsevier, Amsterdam **2006**.
[28] C. A. Hampel, *Encyclopedia of the Chemical Elements*, Reinhold Book Corp, Netherlands **1968**.
[29] L. Gal'chinetskii, S. Galkin, M. Dobrotvorskaya, I. Rybalka, *Adv. Funct. Mater.* **2012**.
[30] We observed experimentally that exposure of ZnSe(ba) to pH 6.8 water reduced its degradation rate; water of pH 7.0 or 7.2 led to more rapid degradation, suggesting that OH^- and not H^+ is critical for LH degradation.
[31] R. Kowalik, P. Żabiński, K. Fitzner, *Electrochim. Acta* **2008**, *53*, 6184.
[32] J. B. Allen, R. F. Larry, *Electrochemical Methods Fundamentals and Applications*, Wiley, New York **2001**.
[33] a) N. J. Nicholas, G. V. Franks, W. A. Ducker, *CrystEngComm* **2012**, *14*, 1232; b) M. Wang, Y. Zhou, Y. Zhang, S. H. Hahn, E. J. Kim, *CrystEngComm* **2011**, *13*, 6024; c) W. Jia, S. Dang, H. Liu, Z. Zhang, C. Yu, X. Liu, B. Xu, *Mater. Lett.* **2012**, *82*, 99; d) G. Otis, M. Ejgenberg, Y. Mastai, *Nanomaterials* **2021**, *11*, 238.
[34] X. Huang, J. Li, *J. Am. Chem. Soc.* **2007**, *129*, 3157.
[35] J. Wang, B. H. Toby, P. L. Lee, L. Ribaud, S. M. Antao, C. Kurtz, M. Ramanathan, R. B. V. Dreele, M. A. Beno, *Rev. Sci. Instrum.* **2008**, *79*, 085105.
[36] A. K. Rappe, C. J. Casewit, K. S. Colwell, W. A. Goddard, W. M. Skiff, *J. Am. Chem. Soc.* **1992**, *114*, 10024.
[37] J. I. Feldblyum, C. H. McCreery, S. C. Andrews, T. Kurosawa, E. J. Santos, V. Duong, L. Fang, A. L. Ayzner, Z. Bao, *Chem. Commun.* **2015**, *51*, 13894.
[38] A. Wexler, S. Hasegawa, *J. Res. Natl. Bur. Stand.* **1954**, *53*, 19.
[39] Y. Shao, Z. Gan, E. Epifanovsky, A. T. B. Gilbert, M. Wormit, J. Kussmann, A. W. Lange, A. Behn, J. Deng, X. Feng, D. Ghosh, M. Goldey, P. R. Horn, L. D. Jacobson, I. Kaliman, R. Z. Khaliullin, T. Kuś, A. Landau, J. Liu, E. I. Proynov, Y. M. Rhee, R. M. Richard, M. A. Rohrdanz, R. P. Steele, E. J. Sundstrom, H. L. Woodcock, P. M. Zimmerman, D. Zuev, B. Albrecht, E. Alguire, et al., *Mol. Phys.* **2015**, *113*, 184.
[40] C. Adamo, V. Barone, *J. Chem. Phys.* **1999**, *110*, 6158.
[41] a) P. J. Hay, W. R. Wadt, *J. Chem. Phys.* **1985**, *82*, 270; b) P. J. Hay, W. R. Wadt, *J. Chem. Phys.* **1985**, *82*, 299.
[42] V. A. Rassolov, J. A. Pople, M. A. Ratner, T. L. Windus, *J. Chem. Phys.* **1998**, *109*, 1223.
[43] a) S. Grimme, S. Ehrlich, L. Goerigk, *J. Comput. Chem.* **2011**, *32*, 1456; b) F. Jensen, *J. Chem. Phys.* **2001**, *115*, 9113.
[44] S. Grimme, J. Antony, S. Ehrlich, H. Krieg, *J. Chem. Phys.* **2010**, *132*, 154104.